

APPLICATION OF TIME-AWARE PC ALGORITHM TO COMPUTE CAUSAL FUNCTIONAL CONNECTIVITY IN ALZHEIMER'S DISEASE FROM FMRI DATA

RAHUL BISWAS* AND SURYANARAYANA SRIPADA**

ABSTRACT. *Functional Connectivity* between brain regions is known to be altered in Alzheimer's disease, and promises to be a biomarker for early diagnosis of the disease. While several approaches for functional connectivity obtain an un-directed network representing stochastic associations (correlations) between brain regions, association does not necessarily imply causation. In contrast, *Causal Functional Connectivity* is more informative, providing a directed network representing causal relationships between brain regions. In this paper, we obtained the causal functional connectome for the whole brain from recordings of resting-state functional magnetic resonance imaging (rs-fMRI) for subjects from three clinical groups: cognitively normal, mild cognitive impairment, and Alzheimer's disease. We applied the recently developed *Time-aware PC* (TPC) algorithm to infer the causal functional connectome for the whole brain. TPC supports model-free estimation of whole brain causal functional connectivity based on directed graphical modeling in a time series setting. We then perform an exploratory analysis to identify the causal brain connections between brain regions which have altered strengths between pairs of subject groups, and over the three subject groups, based on edge-wise p-values from statistical tests. We used the altered causal brain connections thus obtained to compile a comprehensive list of brain regions impacted by Alzheimer's disease according to the current data set. The brain regions thus identified are found to be in agreement with literature on brain regions impacted by Alzheimer's disease, published by researchers from clinical/medical institutions.

Keywords: Causal inference, functional connectivity, brain mapping, directed graphical modeling, Alzheimer's disease, functional magnetic resonance imaging.

1. INTRODUCTION

Alzheimer's disease (AD) is the most common age-related progressive neurodegenerative disorder. It typically begins with a preclinical phase and advances through mild cognitive impairment (MCI) to clinically significant AD, which is a form of dementia (Querfurth and LaFerla, 2010). Despite significant efforts to identify biomarkers for

*DEPARTMENT OF ELECTRICAL AND COMPUTER ENGINEERING, UNIVERSITY OF WASHINGTON, SEATTLE, WA, 98195, USA. *E-mail for correspondence:* rbiswas1@uw.edu.

**CENTER FOR RESEARCH ON SCIENCE AND CONSCIOUSNESS, REDMOND, WA, 98052, USA.

AD, it still relies on clinical diagnosis, and early and accurate prediction of the disease remains limited (Laske et al., 2015; Li et al., 2019). Abnormal resting-state functional connectivity (FC) between brain regions has been observed as early as two decades before brain atrophy and the emergence of AD symptoms (Ashraf et al., 2015; Nakamura et al., 2017). Therefore, resting-state FC can potentially determine the relative risk of developing AD (Brier et al., 2014; Sheline and Raichle, 2013).

Resting-state functional magnetic resonance imaging (rs-fMRI) records the blood-oxygen-level-dependent (BOLD) signal from different brain regions while individuals are awake and not engaged in any specific task. The BOLD signal is popularly used to infer functional connectivity between brain regions partly due to the advantage that BOLD signal provides high spatial resolution (Yamasaki et al., 2012; Sporns, 2013; Liu et al., 2015; Xue et al., 2019).

Functional connectivity refers to the stochastic relationship between brain regions with respect to their activity over time. Popularly, functional connectivity involves measuring statistical association between signals from different brain regions. The statistical association measures are either pairwise associations between pairs of brain regions such as Pearson’s correlation, or multivariate i.e. incorporating multi-regional interactions such as undirected graphical models (Biswas and Shlizerman, 2022a). Detailed technical explanations of functional connectivity in fMRI can be found in Chen et al. (2017); Keilholz et al. (2017); Scarapicchia et al. (2018). The findings from studies using FC (Wang et al., 2007; Kim et al., 2016), and meta-analyses (Jacobs et al., 2013; Li et al., 2015; Badhwar et al., 2017) indicate a decrease in connectivity in several brain regions in relation to Alzheimer’s disease (AD), such as the hippocampus and posterior cingulate cortex. These regions play a role in memory and attentional processing. On the other hand, some studies have found an increase in connectivity within brain regions in early stages of AD and MCI (Gour et al., 2014; Bozzali et al., 2015; Hillary and Grafman, 2017). This is a well known phenomenon, where increase in FC between certain brain regions occurs when the communication between other brain regions is impaired. Such hyperconnectivity has been interpreted as a compensatory mechanism where alternative paths within the brain’s network are recruited (Hillary and Grafman, 2017; Marek and Dosenbach, 2022; Oldham and Fornito, 2019).

In contrast to associative FC, causal FC represents functional connectivity between brain regions more informatively by a directed graph, with nodes as the brain regions, directed edges between nodes indicating causal relationships between the brain regions, and weights of the directed edges quantifying the strength of the corresponding causal relationship (Spirtes et al., 2000). However, functional connectomics studies in general,

and in relation to fMRI from Alzheimer's disease in particular, have predominantly used associative measures of FC (Reid et al., 2019). There are a few studies focusing on alterations in CFC in relation to Alzheimer's disease (Rytsar et al., 2011; Khatri et al., 2021), however this area is largely unexplored. This is partly due to the lack of methods that can infer the CFC in a desirable manner as explained next.

Several properties are desirable in the context of causal modeling of functional connectivity (Biswas and Shlizerman, 2022a; Smith et al., 2011). Specifically, the CFC should represent causality while free of limiting assumptions such as linearity of interactions. In addition, since the activity of brain regions are related over time, such temporal relationships should be incorporated in defining causal relationships in neural activity. The estimation of CFC should be computationally feasible for the whole brain functional connectivity, instead of limiting to a smaller brain network. It is also desirable to capture beyond-pairwise multi-regional cause and effect interactions between brain regions. Furthermore, since the BOLD signal occurs and is sampled at a temporal resolution that is far slower than the neuronal activity, thereby causal effects often appear as contemporaneous (Granger, 1969; Smith et al., 2011). Therefore, the causal model in fMRI data should support contemporaneous interactions between brain regions.

Among the methods for finding CFC, *Dynamic Causal Model* (DCM) requires a mechanistic biological model and compares different model hypotheses based on evidence from data, and is unsuitable for estimating the CFC of the whole brain (Friston et al., 2003; Smith et al., 2011). On the other hand, Granger Causality typically assumes a vector auto-regressive linear model for activity of brain regions over time, and it tells whether a regions's past is predictive of another's future (Granger, 2001). Furthermore, GC does not include contemporaneous interactions. This is a drawback since fMRI data often consists of contemporaneous interactions (Smith et al., 2011). In contrast, *Directed Graphical Modeling* (DGM) has the advantage that it does not require the specification of a parametric equation of the neural activity over time, it is predictive of the consequence of interventions, and supports estimation of whole brain CFC. Furthermore, the approach inherently goes beyond pairwise interactions to include multiregional interactions between brain regions, along with estimation of the cause and effect of such interactions. The *Time-aware PC* (TPC) algorithm is a recent method for computing the CFC based on DGM in a time series setting (Biswas and Shlizerman, 2022b). In addition, TPC also incorporates contemporaneous interactions among brain regions. A detailed comparative analysis of approaches to find causal functional connectivity is provided in Biswas and Shlizerman (2022a,b). With the

development of methodologies such as Time-aware PC, it would be possible to infer the whole brain CFC with the aforementioned desirable properties.

In this paper, we apply the TPC algorithm to infer the causal functional connectivity between brain regions from resting-state fMRI data. By applying the algorithm to the fMRI of subjects, we estimate the subject-specific CFC for all subjects in the dataset. It is noteworthy that different subjects are in different clinical categories: Cognitively Normal (CN), Mild Cognitive Impairment (MCI), and Alzheimer’s Disease (AD). To identify which causal connections differ between brain regions across pairs of clinical categories, we utilize Welch’s t-test, comparing the weights of causal functional connections of subjects for a pair of clinical categories. This analysis reveals the p-values of causal links between brain regions to exhibit differences between subjects in distinct clinical categories, such as with cognitively normal vs. Alzheimer’s disease. Additionally, we employ a Kruskal-Wallis H-test, which is a non-parametric version of ANOVA test, to find p-values of causal links to exhibit differences across subjects of the three clinical categories. These links provide insights into the causal connectivity connections that are relevant in exhibiting differences among the three clinical categories. We then compile a comprehensive list of brain regions impacted by Alzheimer’s disease based on the altered causal links obtained from the current dataset. Notably, the obtained brain regions are consistent with existing literature, with each such publication being a report from a team involving a clinical setting and at least one medical expert, thereby validating the approach.

2. MATERIALS AND METHODS

2.1. Participants. The resting fMRI and demographic data were downloaded from the Harvard Dataverse (<https://doi.org/10.7910/DVN/29352>) (Mascali et al., 2015b). A total of 30 subjects were included in the study: 10 subjects who are cognitively normal (CN), 10 subjects with mild cognitive impairment (MCI), and 10 subjects with Alzheimer’s disease (AD).

In the experiments, general cognitive evaluation of subjects was obtained using the Mini-Mental State Examination (MMSE) (Mascali et al., 2015b). The subjects were age-matched (ANOVA test: $F = 1.5, p > 0.2$) and gender-matched (chi-square test: $\chi^2 = 1.9, p > 0.3$), although subjects with MCI or AD were less educated than subjects in CN group (t-tests: AD vs CN, $t = -4.0, p < 0.001$; MCI vs CN, $t = -2.3, p < 0.05$). As expected, MMSE scores had a significant difference between all pairs of groups (t-tests: AD vs CN, $t = -6.5, p < 0.001$; MCI vs CN, $t = -4.6, p < 0.001$; MCI vs AD: $t = 3.1, p < 0.05$).

TABLE 1. Subject demographic information summary

	CN	MCI	AD
n	10	10	10
Sex (M/F)	7/3	6/4	4/6
Age (years)	66.0 ± 9.6	70.7 ± 7.1	72.3 ± 8.3
Education (years)	14.5 ± 3.0	11.1 ± 3.5	8.6 ± 3.6
MMSE	29.30 ± 0.67	25.8 ± 2.3	21.5 ± 3.7

Entries represent the mean \pm S.D.

Table 1 includes a summary of the participants’ demographic and medical information.

2.2. Image Acquisition. The acquisition of fMRI images was performed using a Siemens Magnetom Allegra scanner. The fMRI images were obtained using an echo planar imaging (EPI) sequence at a field strength of 3.0 Tesla, with a repetition time (TR) of 2.08 seconds, an echo time (TE) of 30 milliseconds, and a flip angle of 70 degrees. The matrix size was 64×64 pixels, there were 32 axial slices parallel to AC-PC plane, in plane resolution was 3×3 mm², slice thickness was 2.5 mm. Resting scans lasted for 7 mins and 20 secs for a total of 220 volumes during which subjects were instructed to keep their eyes closed, to not think of anything in particular and to refrain from falling asleep.

2.3. fMRI Preprocessing. The fMRI pre-processing steps were carried out using the CONN toolbox version 21a, which utilizes the Statistical Parametric Mapping (SPM12), both of which are MATLAB-based cross-platform software (Nieto-Castanon, 2021; Friston et al., 1994). We used the default preprocessing pipeline in CONN, consisting of the following steps in order: functional realignment and unwarp (subject motion estimation and correction), functional centring to (0,0,0) coordinates (translation), slice-time correction with interleaved slice order, outlier identification using Artifact Detection and Removal Tool (ART), segmentation into gray matter, white matter and cerebrospinal fluid tissue, and direct normalization into standard Montreal Neurological Institute (MNI) brain space, and lastly, smoothing using spatial convolution with a Gaussian kernel of 8mm full width half maximum. This pipeline was followed by detrending, and bandpass filtering (0.001-0.1 Hz) to remove low-frequency scanner drift and physiological noise of the fMRI images. The first four time points have been filtered out to remove any artifact.

For the extraction of Regions-Of-Interest (ROIs), the automated anatomical labeling (AAL) atlas was utilized on the preprocessed rs-fMRI dataset (Tzourio-Mazoyer et al., 2002). The list of all regions in AAL atlas is provided in Appendix A along with their

abbreviated, short, and full region names. This specific parcellation method has been demonstrated to be optimal for studying the functional connectivity between brain regions (Arslan et al., 2018). The voxels within each ROI were averaged, resulting in a time series for each ROI.

2.4. Inference of causal functional connectivity: Time-aware PC algorithm.

The Time-aware PC (TPC) Algorithm finds causal functional connectivity between brain regions from time series based on Directed Graphical Models (DGM) (Spirtes et al., 2000; Pearl, 2009; Biswas and Shlizerman, 2022a,b; Biswas and Mukherjee, 2022). While traditional DGM is applicable to static data, TPC extends the applicability of DGM to CFC inference in time series by firstly implementing the Directed Markov Property (DMP) to model causal spatial and temporal interactions in the time series by an unrolled Directed Acyclic Graph (DAG) of the time series. The unrolled DAG consists of nodes (v, t) , for region of interest v and time t , and edge $(v_1, t_1) \rightarrow (v_2, t_2)$ reflecting causal interaction from the BOLD signal in region v_1 at time t_1 to the BOLD signal in region v_2 at time t_2 . The estimation of the unrolled DAG is carried out by first transforming the time series into sequential variables with a maximum time delay of interaction τ , and then applying the Peter-Clark (PC) algorithm to infer the unrolled DAG based on the sequential variables (Kalisch and Bühlman, 2007). TPC then rolls the DAG back to obtain the CFC graph between the regions of interest (see Figure 1) (Biswas and Shlizerman, 2022b). We consider $\tau = 1$ for our analyses, which would include interactions of the BOLD signal between regions of interest with a maximum time delay of 2.08 s, the TR of the fMRI acquisition.

The CFC outcome of this methodology is interpretable in the following manner: An edge from region $i \rightarrow j$ in the CFC estimate represents significant causal interaction from brain region i at preceding times to region j at following times. The model and the approach are non-parametric, meaning that it does not require the specification of a parametric dynamical equation for neural activity. The method captures beyond-pairwise multivariate interactions between brain regions. It also supports estimation of the CFC for the whole brain in a computationally feasible manner. It also allows for time delays in interactions between the brain units as well as the presence of feedback-loops. Furthermore, it has been shown that if the neural activity obeys an arbitrary dynamical process, the model outcome of TPC is consistent with respect to the causal relationships implied by the dynamical process and is predictive of counterfactual queries such as ablation or modulation (Biswas and Shlizerman, 2022b).

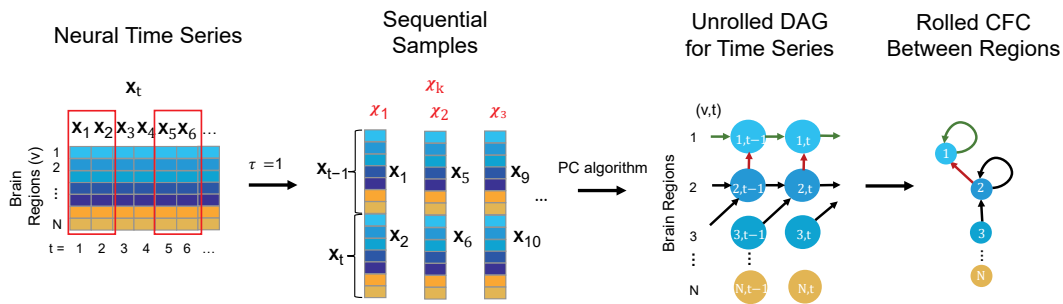


FIGURE 1. Steps conveying the concept of the TPC algorithm to infer CFC from observed neural time series data: First the neural time series is transformed to form sequential samples with a maximum time delay of interaction, τ (here $\tau = 1$). Then, Peter-Clark (PC) algorithm is applied on the sequential samples to obtain the unrolled DAG satisfying the Directed Markov Property. Finally the unrolled DAG is transformed to obtain the Rolled CFC between regions.

It is noteworthy that implementing the DMP on the unrolled DAG to model causal relationships over time enables contemporaneous interactions e.g. from region u to region v at time t (Biswas and Shlizerman, 2022b). Such contemporaneous interactions are represented by the edge $(u, t) \rightarrow (v, t)$ in the unrolled DAG, and presence of such an edge in the unrolled DAG would be reflected as an edge $u \rightarrow v$ in the Rolled CFC outcome. Such contemporaneous interactions are especially relevant in fMRI due to the relatively slow temporal resolution of the BOLD signal compared to the underlying neural activity (Smith et al., 2011).

2.5. Group-wise Comparisons of Estimated CFC. Using the subject-specific CFC estimated by TPC algorithm, we perform further statistical tests. We use Welch's t-test to obtain p-values of connections to exhibit greater or less weight in one disease stage compared to another disease stage (Yuen, 1974). We use the Kruskal-Wallis H-test, which is a non-parametric version of the ANOVA test, to obtain p-values of connections to exhibit unequal weight in either of the four disease stages (Kruskal and Wallis, 1952).

3. RESULTS

3.1. Subject-specific Causal Functional Connectivity. Figure 2 shows the causal functional connectivity (CFC) estimated using TPC algorithm for an example subject in the cognitively normal group. In Figure 2-a, the CFC is represented in the form of a matrix, whose entry (i, j) indicates the presence of connectivity from region index $i \rightarrow j$, and the value at entry (i, j) represents the weight of that causal connection. A positive value (blue) of the weight is indicative of excitatory influence whereas a negative

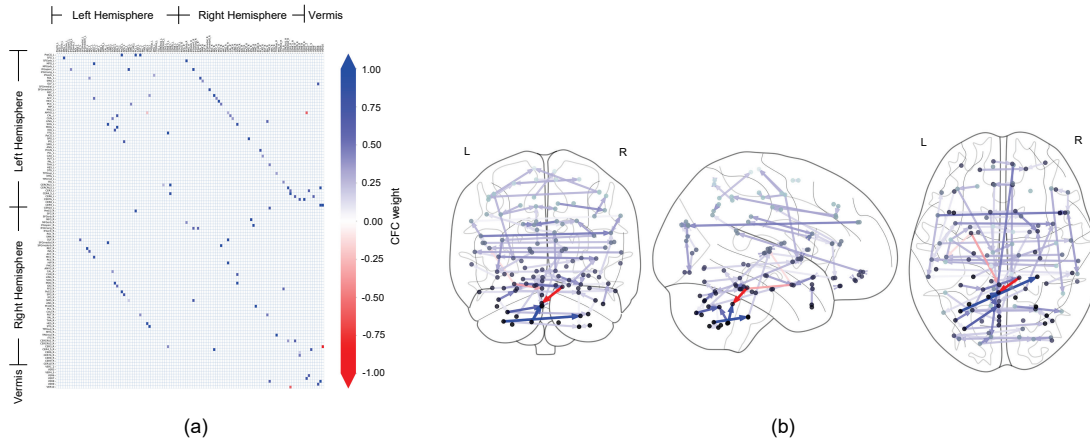


FIGURE 2. CFC outcome of an example subject who is cognitively normal. The CFC is obtained by TPC algorithm. (a) The CFC is represented by a matrix, whose entry (i, j) represents the connection of region $i \rightarrow j$. (b) The CFC is visualized with graph edges on the Frontal, Axial and Lateral brain maps (left to right). The nodes correspond to brain region centers, ranging from superficial (light gray) to deeper (darker gray) regions, in the AAL brain atlas.

value (red) is indicative of inhibitory influence. The diagonal of the matrix representing self-connections for regions has been filtered out. In Figure 2-b, the CFC is represented by a directed graph overlaid on schematics of the brain. The schematics of the brain comprise 2-dimensional brain projections in the Frontal, Axial and Lateral planes. The nodes of the CFC graph correspond to centers of brain regions in the AAL atlas. The nodes are colored light to dark gray according to their depth in the brain, with light gray representing superficial and dark gray representing deeper brain regions. The causal functional connectivity graph provides a highly informative map of causal interactions between brain regions.

3.2. Comparisons of causal functional connectivity over pairwise clinical categories. Figure 3 shows the CFC edges obtained by the TPC algorithm which have p-value less than 0.05 and less than 0.1 for altered (greater/lower) weight between subjects from pairs of disease stages, where the p-values are found by Welch's t-test. This provides insights into which brain connections are impacted by different stages of the disease: healthy, early and late mild cognitive impairment, and Alzheimer's disease.

In Figure 3, the connections with lowest 5 p-values from AD>CN and AD<CN comparisons are: Lobule IV, V of cerebellar hemisphere Left \rightarrow Lobule IV, V of cerebellar hemisphere Right; Superior frontal gyrus, dorsolateral Left \rightarrow Superior frontal

gyrus, medial Left; Middle occipital gyrus Left \rightarrow Middle occipital gyrus Right; Gyrus rectus Right \rightarrow Gyrus rectus Left, Heschl's gyrus Right \rightarrow Heschl's gyrus Left.

3.3. Multi-group comparison of causal functional connectivity. Figure 4 shows the causal functional connections obtained by TPC, which have p-value less than 0.05 and less than 0.1 for difference across either of the four disease stages. Here the p-values are obtained by Kruskal-Wallis H-test. This sheds light on those connections which are impacted during the overall progression of the disease. Here, the connections with lowest 5 p-values are: Lobule VIIB of cerebellar hemisphere Right \rightarrow Crus II of cerebellar hemisphere Right; Lobule IV, V of cerebellar hemisphere Left \rightarrow Lobule IV, V of cerebellar hemisphere Right; Inferior frontal gyrus, pars orbitalis, Right \rightarrow Middle frontal gyrus, pars orbitalis Right; Amygdala Right \rightarrow Hippocampus Right; Lobule VI of cerebellar hemisphere Right \rightarrow Lobule VI of vermis.

3.4. Brain Regions with altered connections. In Table 2, we list 9 brain regions (and 5 additional regions) that correspond to altered causal functional connections to or from them between subjects of CN, MCI and AD groups with edge-wise p-value less than 0.05 (less than 0.1). The subject-specific causal functional connectomes have been estimated using TPC algorithm (see Section 3.2). The brain regions found are in agreement with existing publications cited in Table 2-right column.

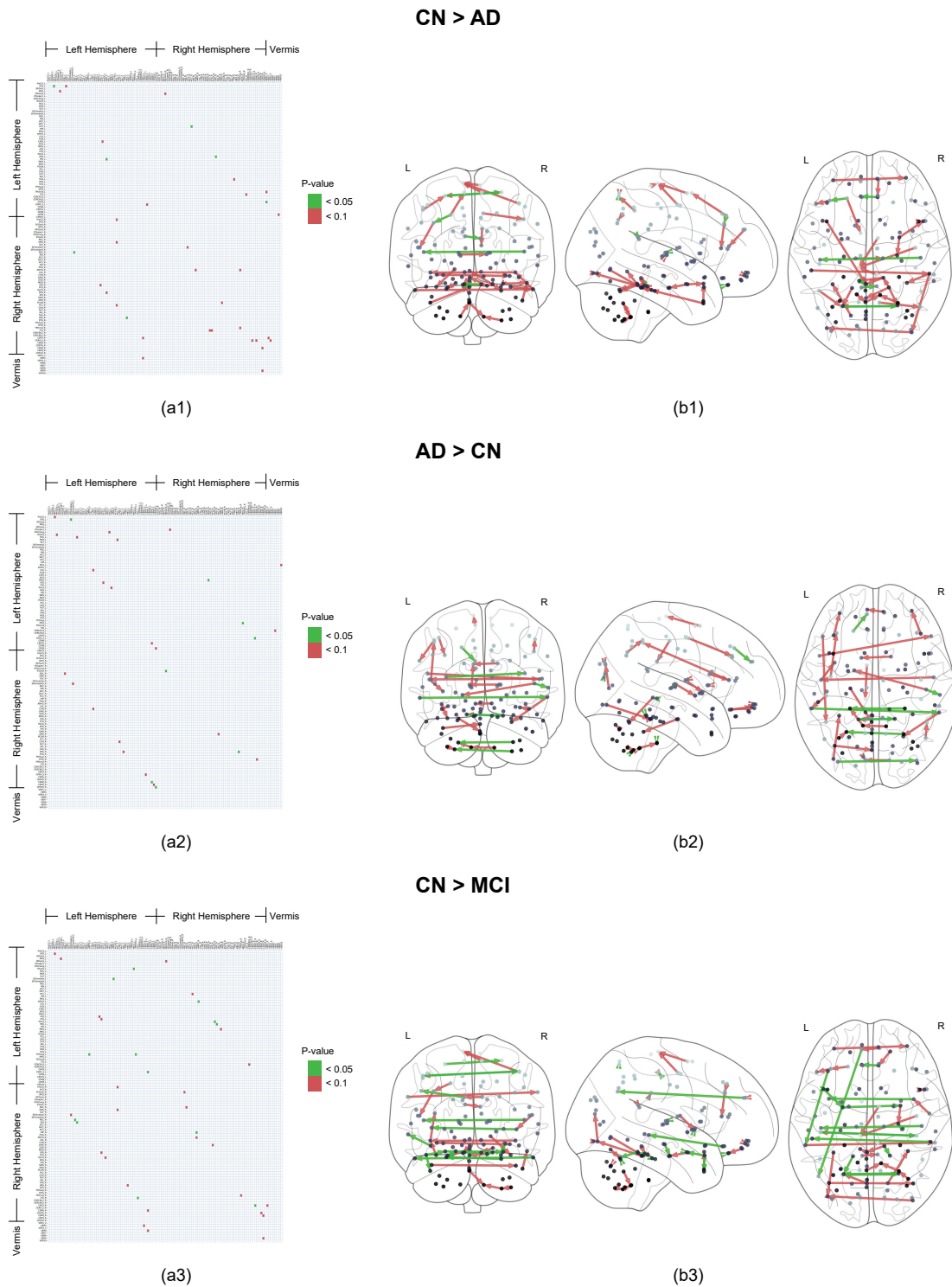


FIGURE 3. Causal functional connections with p-values for altered weights in pairwise comparisons between groups less than 0.05 (green) and less than 0.1 (red), as obtained by Welch's t-test. (a1)-(a3). The connections are represented in matrix format with a non-zero entry in (i, j) corresponding to the edge $i \rightarrow j$. (b1)-(b3). The connections are represented by graph edges on the brain schematics.

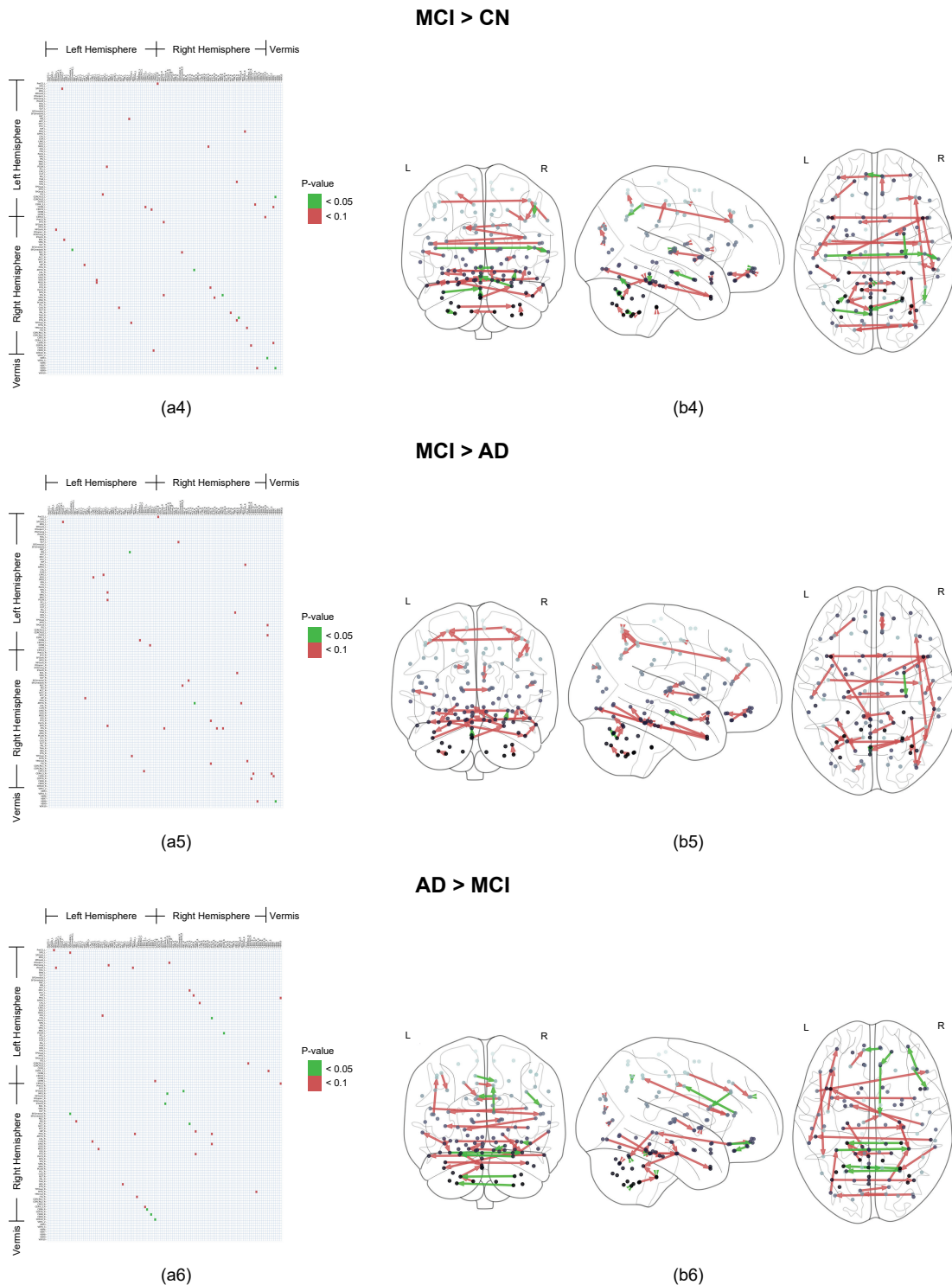


FIGURE 3. (Cont.) Causal functional connections with p-values for altered weights in pairwise comparisons between groups less than 0.05 (green) and less than 0.1 (red), as obtained by Welch's t-test. (a1)-(a3). The connections are represented in matrix format with a non-zero entry in (i, j) corresponding to the edge $i \rightarrow j$. (b1)-(b3). The connections are represented by graph edges on the brain schematics.

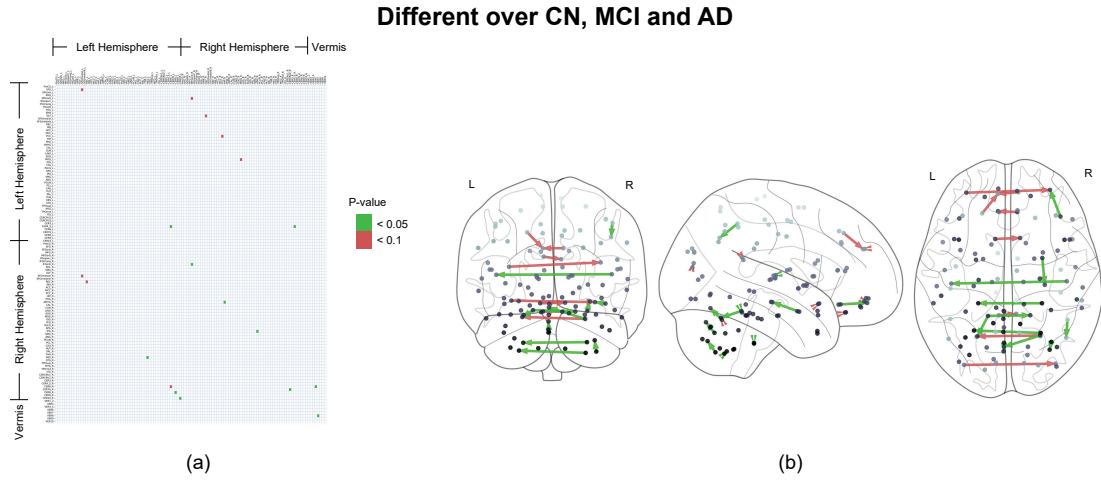


FIGURE 4. Causal functional connections with p-values for altered weights between the three groups of CN, MCI and AD subjects less than 0.05 (green) and additional connections with p-values less than 0.1 (red), where the p-values are obtained by Kruskal-Wallis H-test. (a) The connections are represented in matrix format with a non-zero entry in (i, j) corresponding to the edge $i \rightarrow j$. (b) The connections are represented by graph edges on the schematic of the brain.

Abbreviated Name	Region Name	Reported by
AMYG_R	Amygdala	Vogt et al. (1990); Poulin et al. (2011)
ANG_L, ANG_R	Angular gyrus	Benson et al. (1982); Jagust et al. (2006)
CAU_R	Caudate nucleus	Barber et al. (2002); Madsen et al. (2010)
CER4.5_L, CER4.5_R, CER6_L, CER6_R, CER7b_R, CER8_L, CER8_R, CER10_L, CER10_R, CERCRU2_R, CER6_L, CER6_R	Cerebellum	Joachim et al. (1989); Jacobs et al. (2018)
HES_L, HES_R	Heschl’s gyrus	Hänggi et al. (2011); Dhanjal et al. (2013)
HIP_R	Hippocampus	Ball et al. (1985); Boutet et al. (2014); Rao et al. (2022)
IFGorb_R	Inferior frontal gyrus	Eliasova et al. (2014); Cajanus et al. (2019)
IPG_R	Inferior parietal gyrus	De Reuck et al. (2015); Van Rooden et al. (2015)
MFGorb_R, MFGorb_L	Middle frontal gyrus	Neufang et al. (2011); Zhou et al. (2013)
MTG_R	Middle temporal gyrus	Busatto et al. (2003); Piras et al. (2019)
PCL_L	Paracentral lobule	Garcia Martin et al. (2013); Yang et al. (2019)
VER6, VER7, VER8, VER1.2	Vermis	Sjöbeck and Englund (2001); A Mavroudis et al. (2013)
PCC_L, PCC_R	Cingulate gyrus	Villain et al. (2008); Caminiti et al. (2020); Mascali et al. (2015a)
REC_L, REC_R	Gyrus rectus	Mölsä et al. (1987); Nochlin et al. (1993); Sheline et al. (2010)
MOG_L, MOG_R	Middle occipital gyrus	Golby et al. (2005); Frings et al. (2015)
OLF_L, OLF_R	Olfactory cortex	Reyes et al. (1993); Wang et al. (2010)
SFG_L, SFGmedial_L, SFGmedial_R	Superior frontal gyrus	Brachova et al. (1993); Lue et al. (1996)

TABLE 2. Brain regions corresponding to altered causal functional connections, whose strength is altered between CN, MCI and AD subject groups with p-values less than 0.05 (green) and additionally with p-values less than 0.1 (red) based on Kruskal-Wallis H-test. The causal functional connections are obtained by TPC algorithm.

4. DISCUSSION

In this study, we have obtained the causal functional connectivity of the whole brain from resting state fMRI time series. We used the recently developed Time-aware PC (TPC) algorithm based on directed graphical modeling in time series, to compute the causal functional connectivity. In the dataset, the subjects belonged to three clinical categories: cognitively normal (CN), mild cognitive impairment (MCI) and Alzheimer’s disease (AD). We performed group-wise comparisons of the subject-specific causal functional connectivity to identify which causal functional connections are altered between pairs of subject groups. The altered causal functional connections between CN and AD were used to obtain brain regions involved with such altered connections in AD. This resulted in the identification of 12 brain regions where causal functional connections to or from those regions are altered in Alzheimer’s disease with p-value less than 0.05, and 5 additional regions with p-value less than 0.1.

It is noteworthy that while several studies have concluded decreased connectivity in MCI and AD compared to CN ([Jacobs et al., 2013](#); [Li et al., 2015](#); [Badhwar et al., 2017](#)), prominent researchers have highlighted that MCI and early stages of AD can involve an increase in functional connectivity between brain regions. This increase occurs when the communication between specific brain regions is impaired. It has been interpreted as a compensatory mechanism where alternative paths within the brain’s network are recruited ([Hillary and Grafman, 2017](#); [Marek and Dosenbach, 2022](#); [Oldham and Fornito, 2019](#)). This explains the presence of causal functional connections estimated by TPC algorithm, whose weight in AD is greater compared to CN in addition to connections with weight in AD less than that in CN (see [Figure 3](#)). The following are causal functional connections found by TPC, that have edge-wise p-value less than 0.05 for strength in AD greater than that in CN, and are lowest 5 in p-value: Lobule IV, V of cerebellar hemisphere Left \rightarrow Lobule IV, V of cerebellar hemisphere Right; Superior frontal gyrus, dorsolateral Left \rightarrow Superior frontal gyrus, medial Left; Middle occipital gyrus Left \rightarrow Middle occipital gyrus Right; Middle temporal gyrus Left \rightarrow Middle temporal gyrus Right; Heschl’s gyrus Right \rightarrow Superior temporal gyrus Right.

In the short term, the augmentation of functional connectivity along alternative pathways exhibits efficiency and adaptability of the brain. However, it is imperative to acknowledge the susceptibility of these densely interconnected hubs to beta-amyloid deposition, which can elicit secondary damage through metabolic stress, ultimately culminating in system breakdown ([Hillary and Grafman, 2017](#)). Consequently, the initial state of hyperconnectivity observed in neurodegenerative disorders may gradually

transition into hypoconnectivity among the engaged pathways, thereby contributing to cognitive decline as the disease advances (Marek and Dosenbach, 2022).

Based on the causal functional connectome outcome alone, this study has been able to identify many brain regions related to Alzheimer's disease, which have been reported across more than 30 different studies, using different feature extraction methods and advanced imaging technologies. Therefore, this study demonstrates the promise of a causal functional connectivity approach based on directed graphical models in time series and estimated by TPC algorithm.

Although most of the regions linked to AD have been identified, certain regions such as the Thalamus (Štěpán-Buksakowska et al., 2014), that have been also linked with AD has not been identified by the methodology. This can be due to lack of significance given the low sample size or choice of significance level. However, the study demonstrates the potential in using the methodology to a larger dataset. Using a larger dataset, the causal functional connectomics methodology can be used for 1) computation of a subject's causal functional connectome from their fMRI data, 2) identification of specific connections as biomarkers for Alzheimer's disease, and 3) using biomarker connections for the early prognosis and diagnosis of Alzheimer's disease.

In this paper, we have demonstrated the following: (a) Application of the TPC algorithm to compute whole-brain CFC for each subject, (b) Interpretation of CFC in the context of AD using domain (neuropathological) knowledge, and (c) Exploratory analysis for edge-wise differences and corresponding brain regions with altered connectivity in subjects from pairs of clinical categories (CN, MCI and AD), and among the three clinical categories. The findings are consistent with published medical literature. In summary, our results show the promise of computing the whole-brain CFC from fMRI data using the TPC algorithm to gain prognostic and diagnostic insights.

REFERENCES

- A Mavroudis, I., G Manani, M., Petrides, F., Petsoglou, K., D Njau, S., G Costa, V., and J Baloyannis, S. (2013). Dendritic and spinal pathology of the purkinje cells from the human cerebellar vermis in alzheimer's disease. *Psychiatria Danubina*, 25(3):0–226.
- Arslan, S., Ktena, S. I., Makropoulos, A., Robinson, E. C., Rueckert, D., and Parisot, S. (2018). Human brain mapping: A systematic comparison of parcellation methods for the human cerebral cortex. *Neuroimage*, 170:5–30.
- Ashraf, A., Fan, Z., Brooks, D., and Edison, P. (2015). Cortical hypermetabolism in mci subjects: a compensatory mechanism? *European journal of nuclear medicine and molecular imaging*, 42:447–458.

- Badhwar, A., Tam, A., Dansereau, C., Orban, P., Hoffstaedter, F., and Bellec, P. (2017). Resting-state network dysfunction in alzheimer’s disease: a systematic review and meta-analysis. *Alzheimer’s & Dementia: Diagnosis, Assessment & Disease Monitoring*, 8:73–85.
- Ball, M., Hachinski, V., Fox, A., Kirshen, A., Fisman, M., Blume, W., Kral, V., Fox, H., and Merskey, H. (1985). A new definition of alzheimer’s disease: a hippocampal dementia. *The Lancet*, 325(8419):14–16.
- Barber, R., McKeith, I., Ballard, C., and O’Brien, J. (2002). Volumetric mri study of the caudate nucleus in patients with dementia with lewy bodies, alzheimer’s disease, and vascular dementia. *Journal of Neurology, Neurosurgery & Psychiatry*, 72(3):406–407.
- Benson, D. F., Cummings, J. L., and Tsai, S. (1982). Angular gyrus syndrome simulating alzheimer’s disease. *Archives of Neurology*, 39(10):616–620.
- Biswas, R. and Mukherjee, S. (2022). Consistent causal inference from time series with pc algorithm and its time-aware extension. *arXiv preprint arXiv:2210.09038*.
- Biswas, R. and Shlizerman, E. (2022a). Statistical perspective on functional and causal neural connectomics: A comparative study. *Frontiers in Systems Neuroscience*, 16.
- Biswas, R. and Shlizerman, E. (2022b). Statistical perspective on functional and causal neural connectomics: The time-aware pc algorithm. *PLOS Computational Biology*, 18(11):1–27.
- Boutet, C., Chupin, M., Lehericy, S., Marrakchi-Kacem, L., Epelbaum, S., Poupon, C., Wiggins, C., Vignaud, A., Hasboun, D., Defontaine, B., et al. (2014). Detection of volume loss in hippocampal layers in alzheimer’s disease using 7 t mri: a feasibility study. *NeuroImage: Clinical*, 5:341–348.
- Bozzali, M., Dowling, C., Serra, L., Spano, B., Torso, M., Marra, C., Castelli, D., Dowell, N. G., Koch, G., Caltagirone, C., et al. (2015). The impact of cognitive reserve on brain functional connectivity in alzheimer’s disease. *Journal of Alzheimer’s Disease*, 44(1):243–250.
- Brachova, L., Lue, L.-F., Schultz, J., El Rashidy, T., and Rogers, J. (1993). Association cortex, cerebellum, and serum concentrations of c1q and factor b in alzheimer’s disease. *Molecular brain research*, 18(4):329–334.
- Brier, M. R., Thomas, J. B., Fagan, A. M., Hassenstab, J., Holtzman, D. M., Benzinger, T. L., Morris, J. C., and Ances, B. M. (2014). Functional connectivity and graph theory in preclinical alzheimer’s disease. *Neurobiology of aging*, 35(4):757–768.
- Busatto, G. F., Garrido, G. E., Almeida, O. P., Castro, C. C., Camargo, C. H., Cid, C. G., Buchpiguel, C. A., Furuie, S., and Bottino, C. M. (2003). A voxel-based morphometry study of temporal lobe gray matter reductions in alzheimer’s disease.

- Neurobiology of aging*, 24(2):221–231.
- Cajanus, A., Solje, E., Koikkalainen, J., Lötjönen, J., Suhonen, N.-M., Hallikainen, I., Vanninen, R., Hartikainen, P., de Marco, M., Venneri, A., et al. (2019). The association between distinct frontal brain volumes and behavioral symptoms in mild cognitive impairment, alzheimer's disease, and frontotemporal dementia. *Frontiers in neurology*, 10:1059.
- Caminiti, S., Sala, A., Pilotto, A., Presotto, L., Garibotto, V., D'Amelio, M., Liguori, C., Mercuri, N., Padovani, A., and Perani, D. (2020). Imaging dopamine system transporter activity and connectivity in alzheimer's dementia: Neuroimaging/new imaging methods. *Alzheimer's & Dementia*, 16:e043304.
- Chen, J. E., Rubinov, M., and Chang, C. (2017). Methods and considerations for dynamic analysis of functional mr imaging data. *Neuroimaging Clinics*, 27(4):547–560.
- De Reuck, J., Auger, F., Durieux, N., Deramecourt, V., Cordonnier, C., Pasquier, F., Maurage, C.-A., Leys, D., and Bordet, R. (2015). Topography of cortical microbleeds in alzheimer's disease with and without cerebral amyloid angiopathy: a post-mortem 7.0-tesla mri study. *Aging and disease*, 6(6):437.
- Dhanjal, N. S., Warren, J. E., Patel, M. C., and Wise, R. J. (2013). Auditory cortical function during verbal episodic memory encoding in alzheimer's disease. *Annals of neurology*, 73(2):294–302.
- Eliasova, I., Anderkova, L., Marecek, R., and Rektorova, I. (2014). Non-invasive brain stimulation of the right inferior frontal gyrus may improve attention in early alzheimer's disease: a pilot study. *Journal of the neurological sciences*, 346(1-2):318–322.
- Frings, L., Hellwig, S., Spehl, T. S., Bormann, T., Buchert, R., Vach, W., Minkova, L., Heimbach, B., Klöppel, S., and Meyer, P. T. (2015). Asymmetries of amyloid- β burden and neuronal dysfunction are positively correlated in alzheimer's disease. *Brain*, 138(10):3089–3099.
- Friston, K. J., Harrison, L., and Penny, W. (2003). Dynamic causal modelling. *Neuroimage*, 19(4):1273–1302.
- Friston, K. J., Holmes, A. P., Worsley, K. J., Poline, J.-P., Frith, C. D., and Frackowiak, R. S. (1994). Statistical parametric maps in functional imaging: a general linear approach. *Human brain mapping*, 2(4):189–210.
- Garcia Martin, E., De Hoz, R., Rojas, B., Gil, P., Yubero, R., and Ramirez, J. (2013). Macular nerve-fiber-layer measurement in early stage alzheimer's disease using optical coherence tomography. *Acta Ophthalmologica*, 91.
- Golby, A., Silverberg, G., Race, E., Gabrieli, S., O'Shea, J., Knierim, K., Stebbins, G., and Gabrieli, J. (2005). Memory encoding in alzheimer's disease: an fmri study of

- explicit and implicit memory. *Brain*, 128(4):773–787.
- Gour, N., Felician, O., Didic, M., Koric, L., Gueriot, C., Chanoine, V., Confort-Gouny, S., Guye, M., Ceccaldi, M., and Ranjeva, J. P. (2014). Functional connectivity changes differ in early and late-onset alzheimer’s disease. *Human brain mapping*, 35(7):2978–2994.
- Granger, C. W. (1969). Investigating causal relations by econometric models and cross-spectral methods. *Econometrica: journal of the Econometric Society*, pages 424–438.
- Granger, C. W. (2001). *Essays in econometrics: collected papers of Clive WJ Granger*, volume 32. Cambridge University Press.
- Hänggi, J., Streffer, J., Jäncke, L., and Hock, C. (2011). Volumes of lateral temporal and parietal structures distinguish between healthy aging, mild cognitive impairment, and alzheimer’s disease. *Journal of Alzheimer’s Disease*, 26(4):719–734.
- Hillary, F. G. and Grafman, J. H. (2017). Injured brains and adaptive networks: the benefits and costs of hyperconnectivity. *Trends in cognitive sciences*, 21(5):385–401.
- Jacobs, H. I., Hopkins, D. A., Mayrhofer, H. C., Bruner, E., van Leeuwen, F. W., Raaijmakers, W., and Schmahmann, J. D. (2018). The cerebellum in alzheimer’s disease: evaluating its role in cognitive decline. *Brain*, 141(1):37–47.
- Jacobs, H. I., Radua, J., Lückmann, H. C., and Sack, A. T. (2013). Meta-analysis of functional network alterations in alzheimer’s disease: toward a network biomarker. *Neuroscience & Biobehavioral Reviews*, 37(5):753–765.
- Jagust, W., Gitcho, A., Sun, F., Kuczynski, B., Mungas, D., and Haan, M. (2006). Brain imaging evidence of preclinical alzheimer’s disease in normal aging. *Annals of Neurology: Official Journal of the American Neurological Association and the Child Neurology Society*, 59(4):673–681.
- Joachim, C. L., Morris, J. H., and Selkoe, D. J. (1989). Diffuse senile plaques occur commonly in the cerebellum in alzheimer’s disease. *The American journal of pathology*, 135(2):309.
- Kalisch, M. and Bühlman, P. (2007). Estimating high-dimensional directed acyclic graphs with the pc-algorithm. *Journal of Machine Learning Research*, 8(3).
- Keilholz, S., Caballero-Gaudes, C., Bandettini, P., Deco, G., and Calhoun, V. (2017). Time-resolved resting-state functional magnetic resonance imaging analysis: current status, challenges, and new directions. *Brain connectivity*, 7(8):465–481.
- Khatri, U., Lama, R. K., and Kwon, G.-R. (2021). Diagnosis of alzheimer’s disease using effective connectivity of rs-fmri. In *2021 36th International Technical Conference on Circuits/Systems, Computers and Communications (ITC-CSCC)*, pages 1–4. IEEE.

- Kim, H. J., Cha, J., Lee, J.-M., Shin, J. S., Jung, N.-Y., Kim, Y. J., Choe, Y. S., Lee, K. H., Kim, S. T., Kim, J. S., et al. (2016). Distinctive resting state network disruptions among alzheimer's disease, subcortical vascular dementia, and mixed dementia patients. *Journal of Alzheimer's Disease*, 50(3):709–718.
- Kruskal, W. H. and Wallis, W. A. (1952). Use of ranks in one-criterion variance analysis. *Journal of the American statistical Association*, 47(260):583–621.
- Laske, C., Sohrabi, H. R., Frost, S. M., López-de Ipiña, K., Garrard, P., Buscema, M., Dauwels, J., Soekadar, S. R., Mueller, S., Linnemann, C., et al. (2015). Innovative diagnostic tools for early detection of alzheimer's disease. *Alzheimer's & Dementia*, 11(5):561–578.
- Li, H., Habes, M., Wolk, D. A., Fan, Y., Initiative, A. D. N., et al. (2019). A deep learning model for early prediction of alzheimer's disease dementia based on hippocampal magnetic resonance imaging data. *Alzheimer's & Dementia*, 15(8):1059–1070.
- Li, H.-J., Hou, X.-H., Liu, H.-H., Yue, C.-L., He, Y., and Zuo, X.-N. (2015). Toward systems neuroscience in mild cognitive impairment and alzheimer's disease: A meta-analysis of 75 fmri studies. *Human brain mapping*, 36(3):1217–1232.
- Liu, S., Cai, W., Liu, S., Zhang, F., Fulham, M., Feng, D., Pujol, S., and Kikinis, R. (2015). Multimodal neuroimaging computing: the workflows, methods, and platforms. *Brain informatics*, 2(3):181–195.
- Lue, L.-F., Brachova, L., Civin, W. H., and Rogers, J. (1996). Inflammation, $\alpha\beta$ deposition, and neurofibrillary tangle formation as correlates of alzheimer's disease neurodegeneration. *Journal of neuropathology & experimental neurology*, 55(10):1083–1088.
- Madsen, S. K., Ho, A. J., Hua, X., Saharan, P. S., Toga, A. W., Jack Jr, C. R., Weiner, M. W., Thompson, P. M., Initiative, A. D. N., et al. (2010). 3d maps localize caudate nucleus atrophy in 400 alzheimer's disease, mild cognitive impairment, and healthy elderly subjects. *Neurobiology of aging*, 31(8):1312–1325.
- Marek, S. and Dosenbach, N. U. (2022). The frontoparietal network: function, electrophysiology, and importance of individual precision mapping. *Dialogues in clinical neuroscience*.
- Mascali, D., DiNuzzo, M., Gili, T., Moraschi, M., Fratini, M., Maraviglia, B., Serra, L., Bozzali, M., and Giove, F. (2015a). Intrinsic patterns of coupling between correlation and amplitude of low-frequency fmri fluctuations are disrupted in degenerative dementia mainly due to functional disconnection. *PLOS ONE*, 10(4):1–18.
- Mascali, D., DiNuzzo, M., Gili, T., Moraschi, M., Fratini, M., Maraviglia, B., Serra, L., Bozzali, M., and Giove, F. (2015b). Resting-state fMRI in dementia patients.

- Mölsä, P., Säkö, E., Paljärvi, L., Rinne, J., and Rinne, U. (1987). Alzheimer’s disease: neuropathological correlates of cognitive and motor disorders. *Acta neurologica scandinavica*, 75(6):376–384.
- Nakamura, A., Cuesta, P., Kato, T., Arahata, Y., Iwata, K., Yamagishi, M., Kuratsubo, I., Kato, K., Bundo, M., Diers, K., et al. (2017). Early functional network alterations in asymptomatic elders at risk for alzheimer’s disease. *Scientific Reports*, 7(1):1–11.
- Neufang, S., Akhrif, A., Riedl, V., Förstl, H., Kurz, A., Zimmer, C., Sorg, C., and Wohlschläger, A. M. (2011). Disconnection of frontal and parietal areas contributes to impaired attention in very early alzheimer’s disease. *Journal of Alzheimer’s Disease*, 25(2):309–321.
- Nieto-Castanon, A. (2021). Conn functional connectivity toolbox (rrid: Scr_009550), version 21.
- Nochlin, D., Van Belle, G., Bird, T., and Sumi, S. (1993). Comparison of the severity of neuropathologic changes in familial and sporadic alzheimer’s disease. *Alzheimer disease and associated disorders*, 7(4):212–222.
- Oldham, S. and Fornito, A. (2019). The development of brain network hubs. *Developmental cognitive neuroscience*, 36:100607.
- Pearl, J. (2009). *Causality*. Cambridge university press.
- Piras, I. S., Krate, J., Delvaux, E., Nolz, J., Matthew, D., Mastroeni, D. F., Serrano, G. E., Sue, L. I., Beach, T. G., Coleman, P. D., et al. (2019). Association of aebp1 and nrn1 rna expression with alzheimer’s disease and neurofibrillary tangle density in middle temporal gyrus. *Brain Research*, 1719:217–224.
- Poulin, S. P., Dautoff, R., Morris, J. C., Barrett, L. F., Dickerson, B. C., Initiative, A. D. N., et al. (2011). Amygdala atrophy is prominent in early alzheimer’s disease and relates to symptom severity. *Psychiatry Research: Neuroimaging*, 194(1):7–13.
- Querfurth, H. W. and LaFerla, F. M. (2010). Alzheimer’s disease. *New England Journal of Medicine*, 362(4):329–344.
- Rao, Y. L., Ganaraja, B., Murlimanju, B., Joy, T., Krishnamurthy, A., and Agrawal, A. (2022). Hippocampus and its involvement in alzheimer’s disease: a review. *3 Biotech*, 12(2):55.
- Reid, A. T., Headley, D. B., Mill, R. D., Sanchez-Romero, R., Uddin, L. Q., Marinazzo, D., Lurie, D. J., Valdés-Sosa, P. A., Hanson, S. J., Biswal, B. B., et al. (2019). Advancing functional connectivity research from association to causation. *Nature neuroscience*, 1(10).
- Reyes, P. F., Deems, D. A., and Suarez, M. G. (1993). Olfactory-related changes in alzheimer’s disease: a quantitative neuropathologic study. *Brain research bulletin*,

- 32(1):1–5.
- Rytsar, R., Fornari, E., Frackowiak, R. S., Ghika, J. A., and Knyazeva, M. G. (2011). Inhibition in early alzheimer's disease: an fmri-based study of effective connectivity. *Neuroimage*, 57(3):1131–1139.
- Scarapicchia, V., Mazerolle, E. L., Fisk, J. D., Ritchie, L. J., and Gawryluk, J. R. (2018). Resting state bold variability in alzheimer's disease: a marker of cognitive decline or cerebrovascular status? *Frontiers in aging neuroscience*, 10:39.
- Sheline, Y. I. and Raichle, M. E. (2013). Resting state functional connectivity in preclinical alzheimer's disease. *Biological psychiatry*, 74(5):340–347.
- Sheline, Y. I., Raichle, M. E., Snyder, A. Z., Morris, J. C., Head, D., Wang, S., and Mintun, M. A. (2010). Amyloid plaques disrupt resting state default mode network connectivity in cognitively normal elderly. *Biological psychiatry*, 67(6):584–587.
- Sjöbeck, M. and Englund, E. (2001). Alzheimer's disease and the cerebellum: a morphologic study on neuronal and glial changes. *Dementia and geriatric cognitive disorders*, 12(3):211–218.
- Smith, S. M., Miller, K. L., Salimi-Khorshidi, G., Webster, M., Beckmann, C. F., Nichols, T. E., Ramsey, J. D., and Woolrich, M. W. (2011). Network modelling methods for fmri. *Neuroimage*, 54(2):875–891.
- Spirtes, P., Glymour, C. N., Scheines, R., and Heckerman, D. (2000). *Causation, prediction, and search*. MIT press.
- Sporns, O. (2013). The human connectome: origins and challenges. *Neuroimage*, 80:53–61.
- Štěpán-Buksakowska, I., Szabó, N., Horínek, D., Tóth, E., Hort, J., Warner, J., Charvát, F., Vécsei, L., Rocek, M., and Kincses, Z. T. (2014). Cortical and subcortical atrophy in alzheimer disease: parallel atrophy of thalamus and hippocampus. *Alzheimer disease & associated disorders*, 28(1):65–72.
- Tzourio-Mazoyer, N., Landeau, B., Papathanassiou, D., Crivello, F., Etard, O., Delcroix, N., Mazoyer, B., and Joliot, M. (2002). Automated anatomical labeling of activations in spm using a macroscopic anatomical parcellation of the mni mri single-subject brain. *Neuroimage*, 15(1):273–289.
- Van Rooden, S., Doan, N. T., Versluis, M. J., Goos, J. D., Webb, A. G., Oleksik, A. M., van der Flier, W. M., Scheltens, P., Barkhof, F., Weverling-Rynsburger, A. W., et al. (2015). 7t t2*-weighted magnetic resonance imaging reveals cortical phase differences between early-and late-onset alzheimer's disease. *Neurobiology of aging*, 36(1):20–26.
- Villain, N., Desgranges, B., Viader, F., De La Sayette, V., Mézenge, F., Landeau, B., Baron, J.-C., Eustache, F., and Chételat, G. (2008). Relationships between

- hippocampal atrophy, white matter disruption, and gray matter hypometabolism in alzheimer’s disease. *Journal of Neuroscience*, 28(24):6174–6181.
- Vogt, L. K., Hyman, B., Van Hoesen, G., and Damasio, A. (1990). Pathological alterations in the amygdala in alzheimer’s disease. *Neuroscience*, 37(2):377–385.
- Wang, J., Eslinger, P. J., Doty, R. L., Zimmerman, E. K., Grunfeld, R., Sun, X., Meadowcroft, M. D., Connor, J. R., Price, J. L., Smith, M. B., et al. (2010). Olfactory deficit detected by fmri in early alzheimer’s disease. *Brain research*, 1357:184–194.
- Wang, K., Liang, M., Wang, L., Tian, L., Zhang, X., Li, K., and Jiang, T. (2007). Altered functional connectivity in early alzheimer’s disease: A resting-state fmri study. *Human brain mapping*, 28(10):967–978.
- Xue, C., Yuan, B., Yue, Y., Xu, J., Wang, S., Wu, M., Ji, N., Zhou, X., Zhao, Y., Rao, J., et al. (2019). Distinct disruptive patterns of default mode subnetwork connectivity across the spectrum of preclinical alzheimer’s disease. *Frontiers in Aging Neuroscience*, 11:307.
- Yamasaki, T., Muranaka, H., Kaseda, Y., Mimori, Y., and Tobimatsu, S. (2012). Understanding the pathophysiology of alzheimer’s disease and mild cognitive impairment: A mini review on fmri and erp studies. *Neurology research international*, 2012.
- Yang, H., Xu, H., Li, Q., Jin, Y., Jiang, W., Wang, J., Wu, Y., Li, W., Yang, C., Li, X., et al. (2019). Study of brain morphology change in alzheimer’s disease and amnesic mild cognitive impairment compared with normal controls. *General psychiatry*, 32(2).
- Yuen, K. K. (1974). The two-sample trimmed t for unequal population variances. *Biometrika*, 61(1):165–170.
- Zhou, B., Liu, Y., Zhang, Z., An, N., Yao, H., Wang, P., Wang, L., Zhang, X., and Jiang, T. (2013). Impaired functional connectivity of the thalamus in alzheimer’s disease and mild cognitive impairment: a resting-state fmri study. *Current Alzheimer Research*, 10(7):754–766.

APPENDIX A. AUTOMATED ANATOMICAL LABELING (AAL) ATLAS

The regions in the AAL atlas along with their abbreviated, short and full names are listed in Table 3.

TABLE 3. Names of regions in the AAL Atlas

No	Abbr. Name	Short Name	Full Region Name
1	PreCG_L	Precentral_L	Precentral gyrus Left
2	PreCG_R	Precentral_R	Precentral gyrus Right

3	SFG_L	Frontal_Sup_L	Superior frontal gyrus, dorsolateral Left
4	SFG_R	Frontal_Sup_R	Superior frontal gyrus, dorsolateral Right
5	SFGorb_L	Frontal_Sup_Orb_L	Superior frontal gyrus, pars orbitalis Left
6	SFGorb_R	Frontal_Sup_Orb_R	Superior frontal gyrus, pars orbitalis Right
7	MFG_L	Frontal_Mid_L	Middle frontal gyrus Left
8	MFG_R	Frontal_Mid_R	Middle frontal gyrus Right
9	MFGorb_L	Frontal_Mid_Orb_L	Middle frontal gyrus, pars orbitalis Left
10	MFGorb_R	Frontal_Mid_Orb_R	Middle frontal gyrus, pars orbitalis Right
11	IFGoperc_L	Frontal_Inf_Oper_L	Inferior frontal gyrus, opercular part Left
12	IFGoperc_R	Frontal_Inf_Oper_R	Inferior frontal gyrus, opercular part Right
13	IFGtriang_L	Frontal_Inf_Tri_L	Inferior frontal gyrus, triangular part Left
14	IFGtriang_R	Frontal_Inf_Tri_R	Inferior frontal gyrus, triangular part Right
15	IFGorb_L	Frontal_Inf_Orb_L	Inferior frontal gyrus, pars orbitalis, Left
16	IFGorb_R	Frontal_Inf_Orb_R	Inferior frontal gyrus, pars orbitalis, Right
17	ROL_L	Rolandic_Oper_L	Rolandic operculum Left
18	ROL_R	Rolandic_Oper_R	Rolandic operculum Right
19	SMA_L	Supp_Motor_Area_L	Supplementary motor area Left
20	SMA_R	Supp_Motor_Area_R	Supplementary motor area Right
21	OLF_L	Olfactory_L	Olfactory cortex Left
22	OLF_R	Olfactory_R	Olfactory cortex Right
23	SFGmedial_L	Frontal_Sup_Medial_L	Superior frontal gyrus, medial Left
24	SFGmedial_R	Frontal_Sup_Medial_R	Superior frontal gyrus, medial Right
25	SFGmedorb_L	Frontal_Med_Orb_L	Superior frontal gyrus, medial orbital Left
26	SFGmedorb_R	Frontal_Med_Orb_R	Superior frontal gyrus, medial orbital Right
27	REC_L	Rectus_L	Gyrus rectus Left
28	REC_R	Rectus_R	Gyrus rectus Right
29	INS_L	Insula_L	Insula Left
30	INS_R	Insula_R	Insula Right
31	ACC_L	Cingulum_Ant_L	Anterior cingulate & paracingulate gyri Left
32	ACC_R	Cingulum_Ant_R	Anterior cingulate & paracingulate gyri Right
33	MCC_L	Cingulum_Mid_L	Middle cingulate & paracingulate gyri Left
34	MCC_R	Cingulum_Mid_R	Middle cingulate & paracingulate gyri Right
35	PCC_L	Cingulum_Post_L	Posterior cingulate gyrus Left
36	PCC_R	Cingulum_Post_R	Posterior cingulate gyrus Right
37	HIP_L	Hippocampus_L	Hippocampus Left
38	HIP_R	Hippocampus_R	Hippocampus Right

39	PHG_L	ParaHippocampal_L	Parahippocampal gyrus Left
40	PHG_R	ParaHippocampal_R	Parahippocampal gyrus Right
41	AMYG_L	Amygdala_L	Amygdala Left
42	AMYG_R	Amygdala_R	Amygdala Right
43	CAL_L	Calcarine_L	Calcarine fissure and surrounding cortex Left
44	CAL_R	Calcarine_R	Calcarine fissure and surrounding cortex Right
45	CUN_L	Cuneus_L	Cuneus Left
46	CUN_R	Cuneus_R	Cuneus Right
47	LING_L	Lingual_L	Lingual gyrus Left
48	LING_R	Lingual_R	Lingual gyrus Right
49	SOG_L	Occipital_Sup_L	Superior occipital gyrus Left
50	SOG_R	Occipital_Sup_R	Superior occipital gyrus Right
51	MOG_L	Occipital_Mid_L	Middle occipital gyrus Left
52	MOG_R	Occipital_Mid_R	Middle occipital gyrus Right
53	IOG_L	Occipital_Inf_L	Inferior occipital gyrus Left
54	IOG_R	Occipital_Inf_R	Inferior occipital gyrus Right
55	FFG_L	Fusiform_L	Fusiform gyrus Left
56	FFG_R	Fusiform_R	Fusiform gyrus Right
57	PoCG_L	Postcentral_L	Postcentral gyrus Left
58	PoCG_R	Postcentral_R	Postcentral gyrus Right
59	SPG_L	Parietal_Sup_L	Superior parietal gyrus Left
60	SPG_R	Parietal_Sup_R	Superior parietal gyrus Right
61	IPG_L	Parietal_Inf_L	Inferior parietal gyrus, excluding supramargina...
62	IPG_R	Parietal_Inf_R	Inferior parietal gyrus, excluding supramargina...
63	SMG_L	SupraMarginal_L	SupraMarginal gyrus Left
64	SMG_R	SupraMarginal_R	SupraMarginal gyrus Right
65	ANG_L	Angular_L	Angular gyrus Left
66	ANG_R	Angular_R	Angular gyrus Right
67	PCUN_L	Precuneus_L	Precuneus Left
68	PCUN_R	Precuneus_R	Precuneus Right
69	PCL_L	Paracentral_Lobule_L	Paracentral lobule Left
70	PCL_R	Paracentral_Lobule_R	Paracentral lobule Right
71	CAU_L	Caudate_L	Caudate nucleus Left
72	CAU_R	Caudate_R	Caudate nucleus Right
73	PUT_L	Putamen_L	Lenticular nucleus, Putamen Left
74	PUT_R	Putamen_R	Lenticular nucleus, Putamen Right

75	PAL_L	Pallidum_L	Lenticular nucleus, Pallidum Left
76	PAL_R	Pallidum_R	Lenticular nucleus, Pallidum Right
77	THA_L	Thalamus_L	Thalamus Left
78	THA_R	Thalamus_R	Thalamus Right
79	HES_L	Heschl_L	Heschl's gyrus Left
80	HES_R	Heschl_R	Heschl's gyrus Right
81	STG_L	Temporal_Sup_L	Superior temporal gyrus Left
82	STG_R	Temporal_Sup_R	Superior temporal gyrus Right
83	TPOsup_L	Temporal_Pole_Sup_L	Temporal pole: superior temporal gyrus Left
84	TPOsup_R	Temporal_Pole_Sup_R	Temporal pole: superior temporal gyrus Right
85	MTG_L	Temporal_Mid_L	Middle temporal gyrus Left
86	MTG_R	Temporal_Mid_R	Middle temporal gyrus Right
87	TPOmid_L	Temporal_Pole_Mid_L	Temporal pole: middle temporal gyrus Left
88	TPOmid_R	Temporal_Pole_Mid_R	Temporal pole: middle temporal gyrus Right
89	ITG_L	Temporal_Inf_L	Inferior temporal gyrus Left
90	ITG_R	Temporal_Inf_R	Inferior temporal gyrus Right
91	CERCRU1_L	Cerebellum_Crus1_L	Crus I of cerebellar hemisphere Left
92	CERCRU1_R	Cerebellum_Crus1_R	Crus I of cerebellar hemisphere Right
93	CERCRU2_L	Cerebellum_Crus2_L	Crus II of cerebellar hemisphere Left
94	CERCRU2_R	Cerebellum_Crus2_R	Crus II of cerebellar hemisphere Right
95	CER3_L	Cerebellum_3_L	Lobule III of cerebellar hemisphere Left
96	CER3_R	Cerebellum_3_R	Lobule III of cerebellar hemisphere Right
97	CER4.5_L	Cerebellum_4.5_L	Lobule IV, V of cerebellar hemisphere Left
98	CER4.5_R	Cerebellum_4.5_R	Lobule IV, V of cerebellar hemisphere Right
99	CER6_L	Cerebellum_6_L	Lobule VI of cerebellar hemisphere Left
100	CER6_R	Cerebellum_6_R	Lobule VI of cerebellar hemisphere Right
101	CER7b_L	Cerebellum_7b_L	Lobule VIIB of cerebellar hemisphere Left
102	CER7b_R	Cerebellum_7b_R	Lobule VIIB of cerebellar hemisphere Right
103	CER8_L	Cerebellum_8_L	Lobule VIII of cerebellar hemisphere Left
104	CER8_R	Cerebellum_8_R	Lobule VIII of cerebellar hemisphere Right
105	CER9_L	Cerebellum_9_L	Lobule IX of cerebellar hemisphere Left
106	CER9_R	Cerebellum_9_R	Lobule IX of cerebellar hemisphere Right
107	CER10_L	Cerebellum_10_L	Lobule X of cerebellar hemisphere Left
108	CER10_R	Cerebellum_10_R	Lobule X of cerebellar hemisphere Right
109	VER1_2	Vermis_1_2	Lobule I, II of vermis
110	VER3	Vermis_3	Lobule III of vermis

111	VER4.5	Vermis_4_5	Lobule IV, V of vermis
112	VER6	Vermis_6	Lobule VI of vermis
113	VER7	Vermis_7	Lobule VII of vermis
114	VER8	Vermis_8	Lobule VIII of vermis
115	VER9	Vermis_9	Lobule IX of vermis
116	VER10	Vermis_10	Lobule X of vermis
